Supplementary Material

1 Supplementary Methods

Materials and reagents

All chemicals and reagents were purchased from Sigma-Aldrich (USA), including the Protran® premium nitrocellulose membranes and dialysis tubing (GE10600003 and D6191 respectively), unless otherwise specified. ELISA plates, Nickel-nitriloacetic acid beads (Ni-NTA), PNGase F and mouse anti-His6 antibody were purchased from Thermofisher (C96 Maxisorp Nunc_Immunoplate, HisPur™, A39245 and MA1-134 respectively, USA). Negative stain EM grids, 200 mesh continuous carbon EM grids, were purchased from (Electron Microscopy Sciences, USA). Uranyl formate was obtained from SPI-Chem (16984-59-1, USA). Human IgG was kindly supplied by Leendert Trouw (IgG1, Alemtuzumab, LUMC). CRP and the spin filters were purchased from Merck (236608 and UFC9010, USA). Anti-human C1 and horseradish peroxidase (HRP) conjugated goat anti-rabbit and goat anti-mouse antibodies were purchased from Dako (Denmark, A013602 P044801, and P044701 respectively). Laemmli buffer 2× and Clarity ECL™ substrate were from Bio-rad (1610737EDU and 1705060 respectively, USA). Goat anti-human C4 and normal human serum (NHS) were purchased from complement technologies (A205 and NHS respectively, USA) and donkey HRP conjugated anti-goat was purchased from Invitrogen (PA1-28664, USA). Octet® streptavidin (SA) biosensors were purchased from Sartorius (Germany). CryoEM grids, specifically Quantifoil 400 mesh grids with holes sizes of 1.2/1.3 µm and a graphene oxide film, were purchased from Aurion (GOQ400R1213Cu10, Netherlands). For sialic acid cleavage, α2-3,6,8,9 neuraminidase A was purchased from New England Biolabs (P0720, USA).

PTX3 expression

A codon-optimised gene construct with the following sequence was ordered from GeneArt, and encoded the PTX3 protein preceded by a signal sequence (bold), and His6-tag and TEV-tag (underlined).

MEFGLSWVFLVALLRGVQCHHHHHHENLYFQGENSDDYDLMYVNLDNEIDNGLHPTEDPT
PCACGQEHSEWDKLFIMLENSQMRERMLLQATDDVLRGELQRLREELGRLAESLARPCAP
GAPAEARLTSALDELLQATRDAGRRLARMEGAEAQRPEEAGRALAAVLEELRQTRADLHA
VQGWAARSWLPAGCETAILFPMRSKKIFGSVHPVRPMRLESFSACIWVKATDVLNKTILF
SYGTKRNPYEIQLYLSYQSIVFVVGGEENKLVAEAMVSLGRWTHLCGTWNSEEGLTSLWV
NGELAATTVEMATGHIVPEGGILQIGQEKNGCCVGGGFDETLAFSGRLTGFNIWDSVLSN
EEIRETGGAESCHIRGNIVGWGVTEIQPHGGAQYVS

The gene was cloned into a pcDNA3.3 expression vector using HindIII and EcoRI restriction sites flanking the construct and correct insertion was checked by Sanger sequencing at the Leiden Genome Technology Center. PTX3 protein was produced by transfecting 25 µg plasmid DNA into Expi293F™ cells in Expi293™ Expression Medium using Opti-MEM and the ExpiFectamine™ 293 Transfection Kit (all ThermoFisher, USA) according the manufacturer's instructions. Supernatant containing PTX3 was harvested 5-7 days post-transfection, centrifuged to remove cellular debris and filtered sequentially through 0.45 µm and 0.2 µm filters (Cytiva, USA).

Purification of PTX3

All steps for protein purification were performed at 4°C unless otherwise stated. For samples used for cryoEM experiments, cellular supernatant was concentrated in a 10 kDa cut off spin filter and buffer exchanged into Tris-HCl 20 mM, NaCl 500 mM, pH 8.0 (buffer A). This was then diluted 5× in buffer A supplemented with 20 mM imidazole. Next, the sample was incubated with a slurry consisting of 2 ml Ni-NTA beads for 30 mins on a gravity flow column. This was then washed with four column volumes of 20 mM, 50 mM and then 70 mM imidazole in buffer A. The protein was eluted using buffer A with 90 mM and 500 mM of imidazole. The resulting eluate was then combined and concentrated in a 10 kDa molecular weight cut-off spin filter and analysed via PAGE and Western blot.

For biochemical experiments, cellular supernatant was dialysed in 12 kDa molecular weight cut-off dialysis tubing against buffer A for four hours and then overnight at in 2 L and 5 L of buffer, respectively. Next, the dialysed supernatant was supplemented with 16 mM imidazole, then added to 5 ml of Ni-NTA beads and incubated overnight on a rotor. This was then added to a gravity flow column and washed with 10 column volumes of buffer A with 30 mM, 50 mM and 70 mM of imidazole, respectively. The protein was eluted with buffer A containing 100 mM, 250 mM and 500 mM imidazole. Fractions were analysed using SDS-PAGE and those containing PTX3 were dialysed overnight against 3 L of Tris buffered saline (TBS; Tris-HCl 50 mM, NaCl 150 mM, pH 7.5). Subsequently, the protein was further purified using SEC with an S200 column (24 ml bed volume, Cytiva, USA). Fractions were analysed using SDS-PAGE and Western blot, as well as their ability to activate complement via ELISA. Quality control was carried out on a S200 increase SEC column (2.4 ml bed volume, Cytiva, USA).

CryoEM sample preparation

PTX, at concentrations between 1-2 µM in 20 mM Tris-HCl, 500 mM NaCl, pH 8.0 was concentrated in a 50 kDa molecular weight cut-off spin filter to concentrations between 60-70 µM, before Tween 20 was added to a final concentration of 0.05% (w/v). For sample preparation multiple conditions were tested, with an optimal particle distribution obtained using 3 µl of PTX3 added to non-glow discharged Quantifoil graphene oxide grids with a 400 mesh copper support and holes sizes of 1.2/1.3 µm. Grids were blotted for 3 seconds with Whatman No. 1 filter paper after a preblot incubation on the grid of 60 seconds, using a Leica EMGP with a chamber environment at 4°C and 65% humidity, before plunge freezing in liquid ethane.

CryoEM data collection

Gain normalised mrc stacks (mrcs format) were collected on a Titan Krios microscope (ThermoFisher) at the Netherlands Centre for Electron Nanoscopy operated at 300 keV and equipped with a Gatan K3 detector and Gatan BioQuantum K3 energy filter with a slit width of 20 eV. Movies were acquired using a total dose of 50 e/Å2 with 50 frames, at 105,000× magnification with a calibrated pixel size of 0.836 Å in super resolution mode (0.418 Å/pix) and a defocus range of -0.8 to -2.0 µm.

CryoEM data analysis

Motion correction and CTF estimation of the micrographs were performed on-the-fly using WARP (1). Particles were picked from motion-corrected micrographs using the neural network within EMAN2 (2). All subsequent steps for producing the final high-resolution map were carried out in Relion 3.1 (3), unless otherwise stated. Particle coordinates were imported, binned 4× and extracted with a box size of 64 pixels, yielding a stack of 1,335,118 particles. The particles were subjected to 2D classification, and classes representing contamination or noise were discarded. An initial model was generated with C4 symmetry applied and used as the reference map for a round of 3D classification. This yielded two higher resolution classes representing a "pyramid" and a "cube" (**Fig. S2**). Both were extracted and binned 2× with a box size of 128 pixels before another round of 2D classification. Poorly aligned classes or classes representing contamination or noise were discarded resulting in 652,097 and 276,374 particles for the pyramid and cube respectively. The particles belonging to the cube class from these 2D classes were also later used in 2D analysis of the N-terminal domains (see below). These particles were then refined with C1 symmetry using their respective 3D classes as reference maps. The particles belonging to the pyramid class were determined to be an artifact resulting from preferential orientation and were not used in subsequent steps (**Fig. S2**). The particles from the cube class were then extracted without binning with a box size of 360 pixels, then refined as before and subsequently subject to three iterations each of beam tilt, anisotropic magnification and per particle defocus. These particles were then refined with C1 symmetry using the previous refinement as a reference map. The model was then aligned to the D4 symmetry axes using relion_image_handler in the command line. The map was then refined using the centred map as a reference, but with D4 symmetry applied. The particles were then polished and refined again with both C1 and D4 symmetry separately. No duplicates were detected, defined as particles within 35 Å of each other.

Enzyme-linked immunosorbent assay (ELISA)

ELISAs were performed using 96 well microtiter plates coated with 50 µl of PTX3 at 10 µg/ml in 0.1 M sodium carbonate (pH 9.3). For coating controls, only the sodium carbonate solution was added. These were incubated for one hour at 37°C, then washed three times in phosphate buffered saline (PBS) with 0.05% Tween 20. Subsequently, wells were blocked with 100 µl of 0.1 M spermidine, before being incubated and washed as previously described. Next, 50 µl NHS or heat inactivated serum (HIS, NHS heated at 56°C for 30 minutes) were diluted in RPMI, added at the concentration ranges described in the figure legends and incubated for one hour at 37°C before washing. To detect C1 or C4 deposition, 50 µl of a rabbit polyclonal anti-human C1q or a goat polyclonal anti-human C4 at a 1:1000 and a 1:150,000 dilution respectively and incubated for one hour before being washed as described above. Thereafter, 50 µl of a goat anti-rabbit or donkey anti-goat antibody conjugated to HRP were added, then incubated for one hour and washed. Absorbance at 415 nm was measured 60 minutes after addition of 50 µl of 2.5 mg/ml 2,2'-azino-bis(3-ethylbenzothiazoline-6-sulfonic acid) (ABTS) in citric acid buffer (0.15 M, pH 4.2) with 0.015% (v/v) H_2O_2 using a Clariostar plus plate reader (BMG Labtech, Germany). Background was taken as the 0% serum well for each condition and subtracted out. Each data point was normalised to the highest value on the plate, specifically 3% NHS with C4 detection. Error bars represent standard deviation of three independent plates.

Octet C1q binding

PTX3 was biotinylated with a 40:1 ratio of biotin to PTX3 with the pierce antibody biotinylation kit (Thermofisher, USA) following the manufacturer's instructions. All steps on the Octet Red385 (Sartorius, Germany) were carried out at 30°C and 1000 rpm. Streptavidin chips were first equilibrated in reaction buffer (tris 50 mM NaCl 150 mM $CaCl_2$ 2 mM Tween 20 0.02% BSA 0.1% pH 7.5) for 10mins. Next sensors were baselined for 120 seconds in reaction buffer, before being put into solutions of 100 or 0 nM biotinylated PTX3 for 120 seconds. The sensors were then baselined again as before, before being exposed to wells with 40-0 nM of pure full C1 complex (Complement Technology, USA) for 300 seconds. Dissociation was then measured for 300 seconds in the same wells used to baseline the sensors. A sensor with no loaded PTX3 and exposed to the highest concentration of C1 were used as a measure of non-specific binding. Data was fitted globally with linked R_{Max} using a 1:1 binding model.

Thermal shift assay

PTX3, CRP or IgG-1 was added at 1 µM in tris buffered saline (TBS, tris 50 mM, NaCl 150 mM, pH 7.4) into capillary tubes and inserted into a Tycho NT.6 as per the manufacturer's instructions. Subsequently, the temperature increased from 35 to 95°C whilst measuring the ratio of 355/330 nm fluorescent signal. Measurements were done in triplicate.

Negative stain tomography

First, 6 µl of PTX3 at 40 µg/ml was applied to continuous-carbon EM grids (200 mesh EM grids, Electron Microscopy Sciences, USA) and incubated for 1 minute. Excess liquid was then removed with filter paper (Whatman, Merck, USA), before 10 µl of uranyl formate (2%) was added to stain for 10 seconds, before excess stain was removed with filter paper. Samples were left to air-dry before being imaged on an FEI Tecnai 12 Twin Transmission electron microscope (ThermoFisher, USA) with a LaB_6 filament operating at 120 kV. Tilts series were acquired with a defocus of ~4 µm on an Eagle 4k x 4K CCD camera (ThermoFisher), at a magnification of ×49000 using a discontinuous tilt scheme from -50° to 50° in 4° increments. Tomograms were reconstructed in IMOD using patch clamp tracking and subsequent weighted back projections with a SIRT like filter.

Modelling glycan interactions

Monosaccharides were added using ISOLDE (54), and joined into a polysaccharide chain in ChimeraX (4) to form a biantennary chain of five N-acetylglucosamine (NAG), six mannose units (MAN), a single fucose (FUC) and one terminal sialic acid (SIA), with the latter occupying the terminal position of one branch (**Fig. S8D,E,F**). This was then manually moved in Isolde to be adjacent to residues of interest whilst the simulation was running and allowed to reach equilibrium. Figures were prepared using ChimeraX (4).

2 Supplementary Figures and Tables

2.1 Supplementary Figures

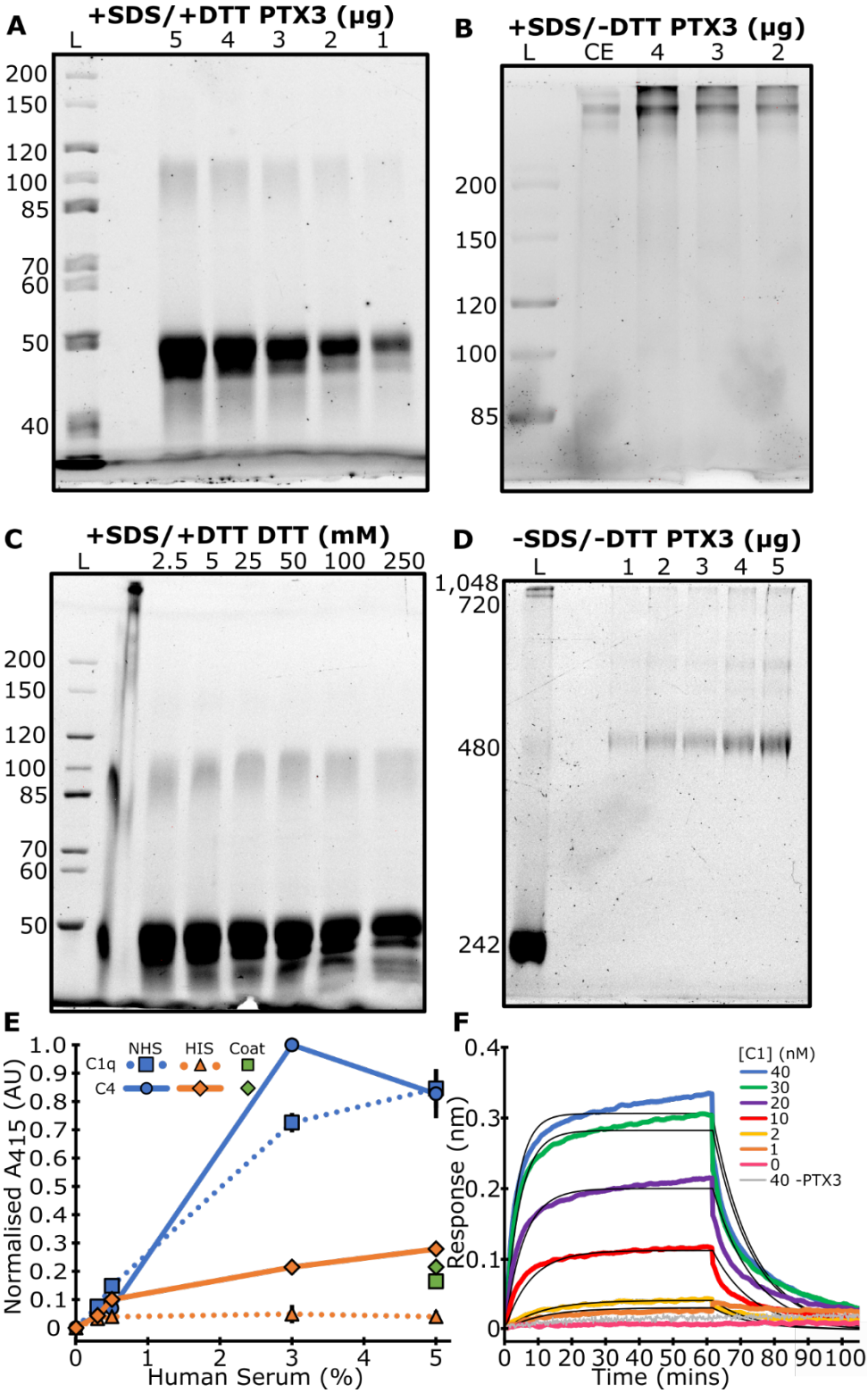

Figure S1. Uncropped gels from Fig. 1 in the main text, DTT titration against PTX3 as well as complement activation and C1 binding by PTX3. (**A**) PTX3 at amounts ranging from 1-5 µg in the

presence of both SDS and DTT, run on a 3-8% gel. (**B**) Pure PTX3 from 2-4 μg, as well as the cell extract (CE) used for purification, in the presence of SDS but not DTT, run on a 3-6% gel. (**C**) PTX3 at 5 μg in the presence of SDS, exposed to various DTT concentrations from 2.5 – 250 mM, run on a 3-8% gel. (**D**) PTX3 from 1-5 μg under native conditions; in the absence of both SDS and DTT, run on a 3-6% gel. Masses in kDa are shown next to the ladder. (**E**) ELISA assays showing PTX3 based complement activation via binding of C1q (dotted line) and deposition of C4 (solid line) when incubated with normal human serum (NHS, blue) but not heat inactivated serum (HIS, orange). NHS (5%) added to the spermidine coat without PTX3 is shown in green. (**F**) Bio-layer inferometry analysis of the binding between biotinylated PTX3 conjugated to streptavidin chips with purified C1 complex. Coloured lines are the raw data traces with concentrations of the C1 complex from 0 – 40 nM. The grey trace represents the maximum concentration of C1 used (40 nM) with no PTX3 loaded onto the chip and the black lines represent the fit of a 1:1 binding model.

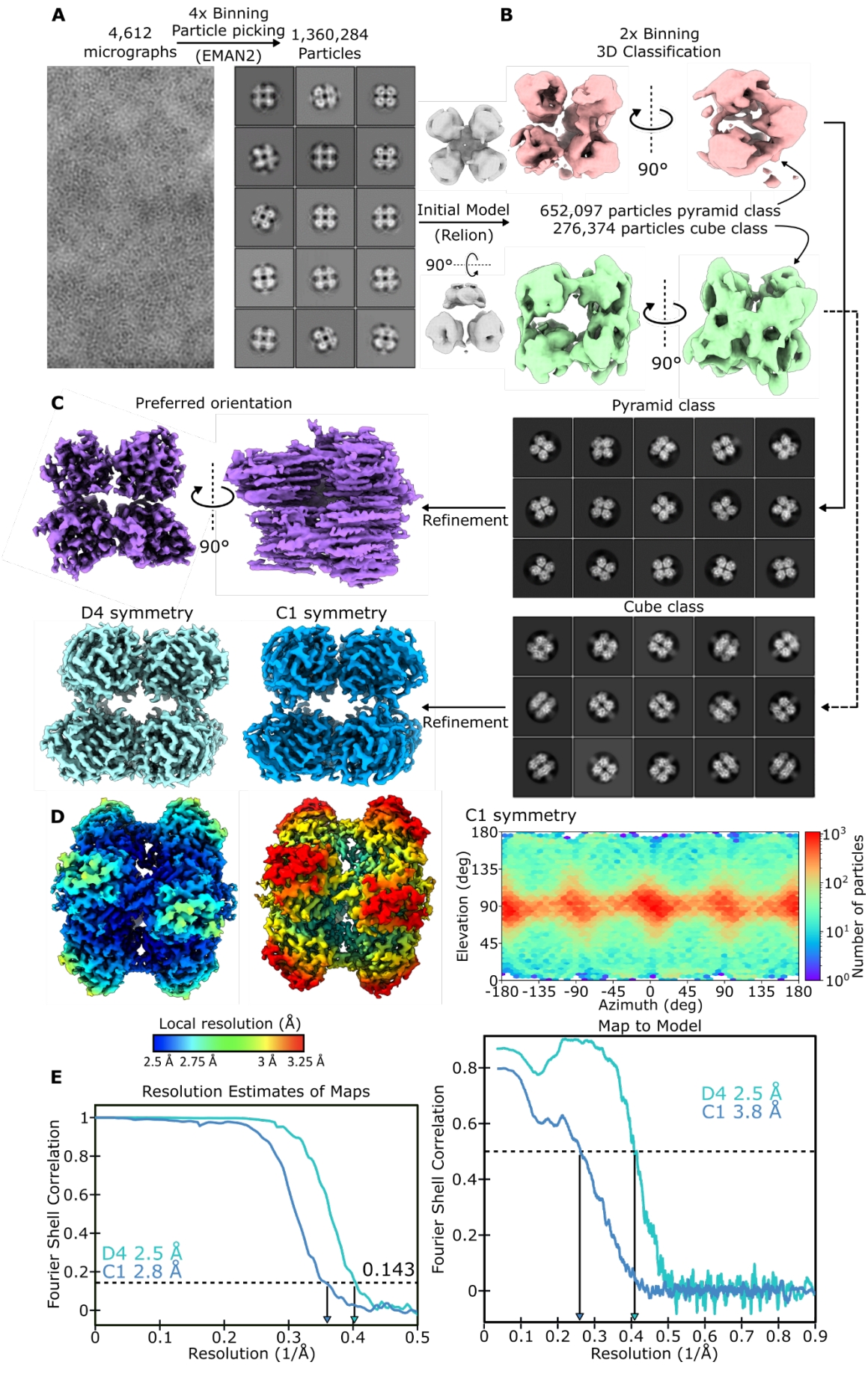
A
4,612 micrographs
4x Binning
Particle picking (EMAN2)
1,360,284 Particles
B
2x Binning
3D Classification
90°
Initial Model (Relion)
652,097 particles pyramid class
276,374 particles cube class
90°
90°
C
Preferred orientation
90°
Refinement
Pyramid class
Cube class
Refinement
D4 symmetry
C1 symmetry
D
C1 symmetry
Elevation (deg)
Azimuth (deg)
Number of particles
Local resolution (Å)
2.5 Å 2.75 Å 3 Å 3.25 Å
E
Resolution Estimates of Maps
Fourier Shell Correlation
D4 2.5 Å
C1 2.8 Å
0.143
Resolution (1/Å)
Map to Model
D4 2.5 Å
C1 3.8 Å
Fourier Shell Correlation
Resolution (1/Å)

Figure S2. Cryo-electron microscopy (CryoEM) data processing. (**A**) EMAN2 was used to pick particles on micrographs of PTX3 on graphene oxide supports. These were binned by 4× and then used to make an initial model with C4 symmetry applied. (**B**) 3D classification with a 2× binned particle stack suggested two subpopulations of pyramid and cube like structures. (**C**) 2D classification and high-resolution refinements revealed the that the pyramid class was in fact octameric PTX3 with preferred orientation. The cube class led to high resolution maps with both D4 and C1 symmetry applied. (**D**) Local resolution and orientations of particles contributing to the final maps. (**E**) Map, and map-to-model, FSC curves of both D4 and C1 maps. Please see the relevant materials and methods section in the main text for more details.

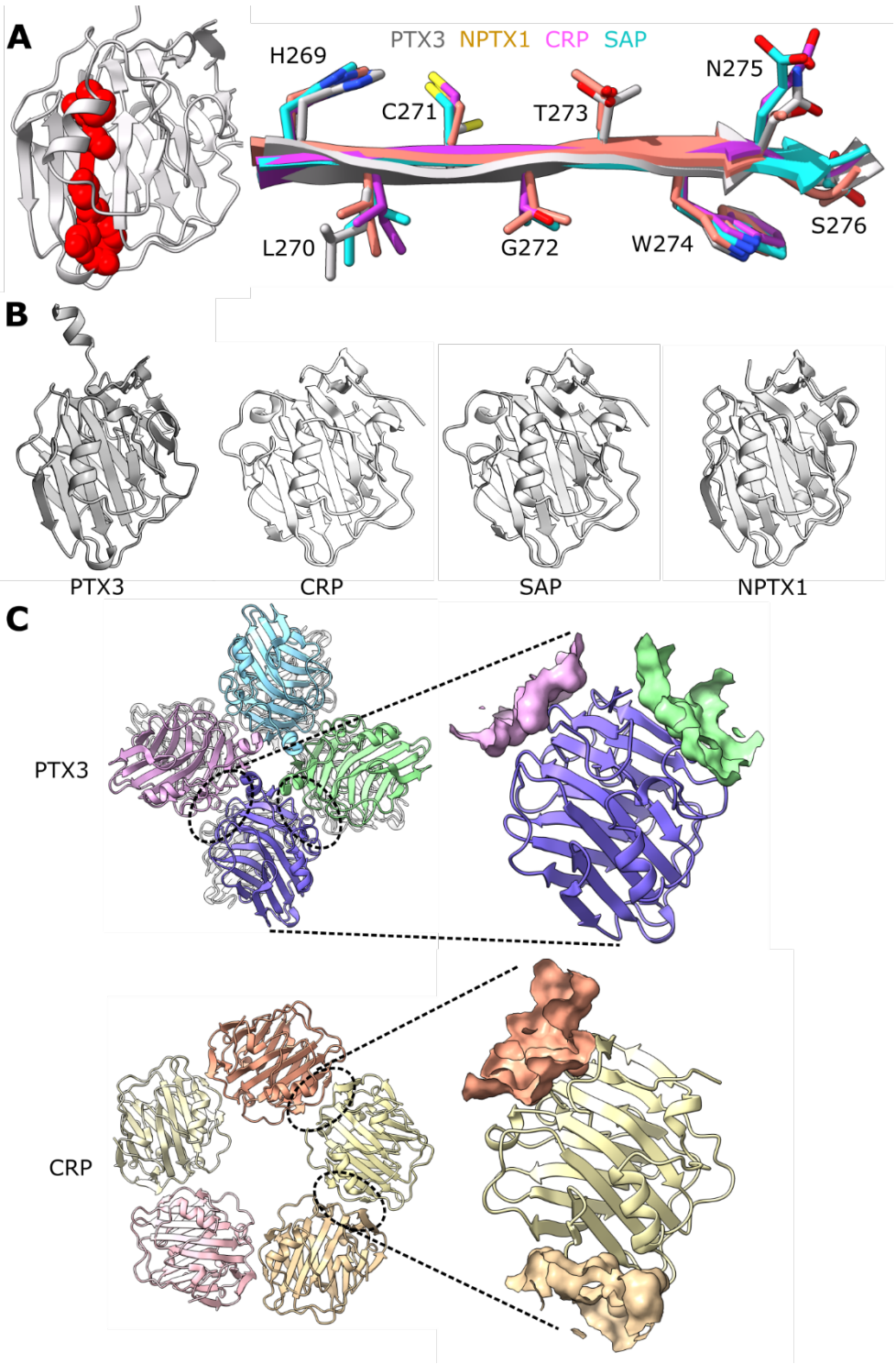

Figure S3. Comparing PTX motifs, domain structures and interfaces. (**A**) PTX domain of PTX3 (grey) shown with the pentraxin sequence highlighted with red spheres. Pentraxin sequence of PTX3 (grey), NPTX1 (orange; PDB code 6YPE), CRP (purple; PDB code 7PKB) and SAP (cyan; PDB code 1SAC) overlaid. (**B**) PTX domains from the structures of the human pentraxins solved so far. (**C**) Planar PTX domain interfaces in PTX3 (top) and CRP (bottom). PTX domains on the right are viewed from the same orientation and the inter-monomer interfaces shown as surfaces.

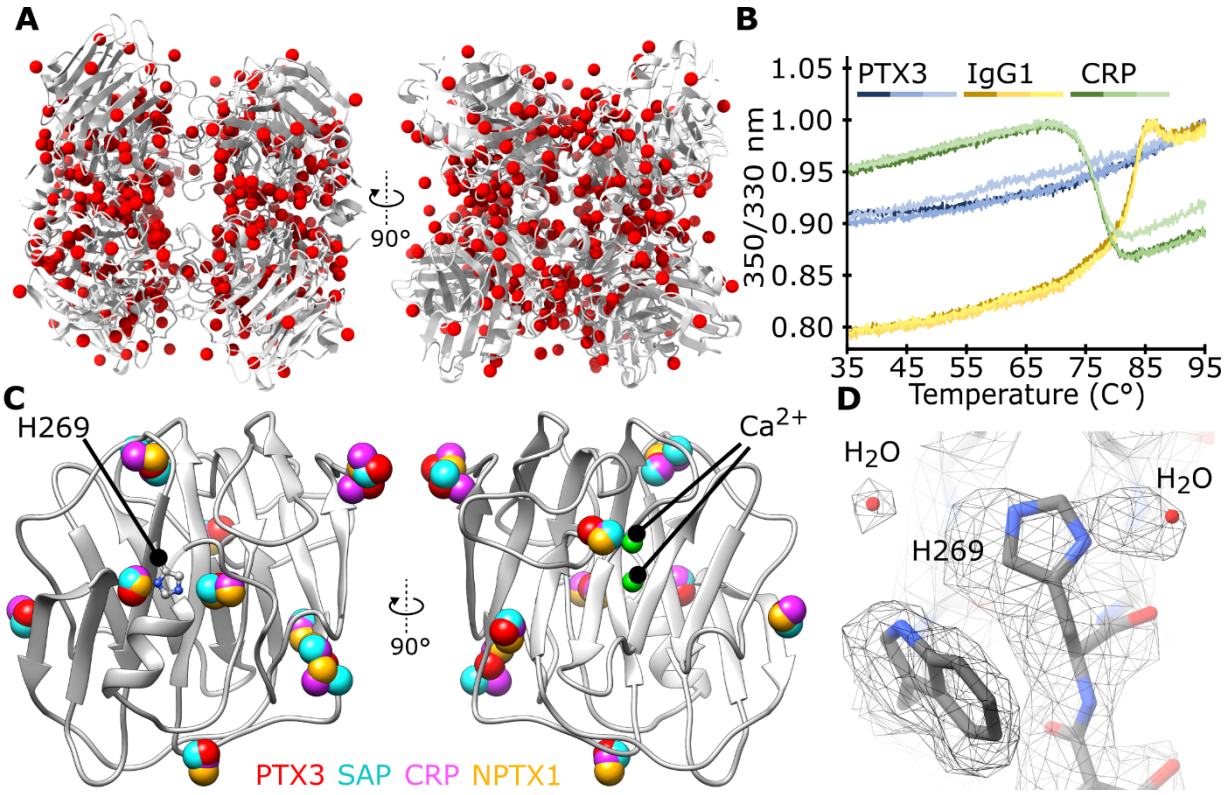

Figure S4. Ordered water molecules of PTX3, enhanced thermostability and ordered water molecules conserved in human pentraxins. (**A**) Ordered water molecules highlighted (red spheres) in and around the PTX domain of PTX3 (grey). (**B**) Thermal shift assay shown in triplicate comparing thermostability of PTX3 (blue), IgG1 (yellow) and CRP (green). (**C**) Identical conserved water molecules in PTX3 (grey), SAP (cyan), CRP (purple) and NPTX1 (orange). Also shown are His269 in PTX3, and the location of Ca^{2+} ions found in CRP, SAP and NPTX1. (**D**) Ordered water molecules found proximal to His269. PTX3 numbering shown for all residues.

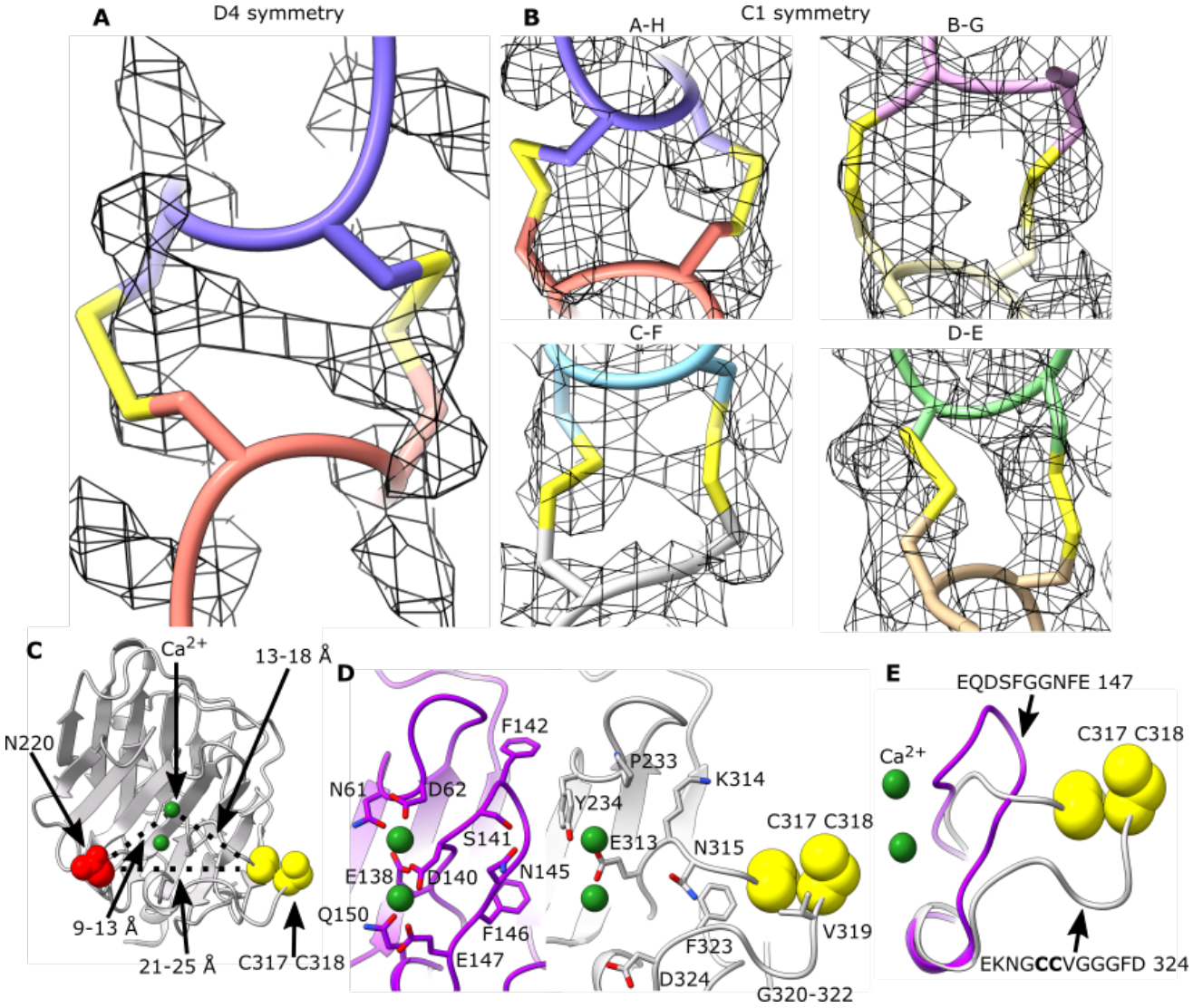

Figure S5. Location, heterogeneity and conservation of the C317-C318 loop. (**A**) Location of the C317 and C318 bonds on the PTX3 octamer. (**A** & **B**) Heterogeneity at positions C317 and C318 in D4 (**A**) and C1 (**B**) refined maps. (**C**) Location of the glycosylated N220 residue (red sphere), Ca^{2+} ions from CRP (green sphere; PDB code 7PKB) and disulfide patch of C317 and C318 (yellow spheres), as well as the distances between the three clusters. (**D**) Enlarged view of residues at the CRP (purple; PDB code 7PKB) Ca^{2+} binding site (green spheres) next to the homologous region in PTX3 (grey) containing the disulfide patch (C317 C318; yellow spheres). Calcium ions are not present in PTX3 but their homologous locations in CRP are mapped on for clarity. (**E**) Superimposition of the Ca^{2+} binding loop in CRP (purple) and loop containing C317 and C318 in PTX3 (grey). Sequences of the loops are shown with the C317 and C318 highlighted in bold for PTX3.

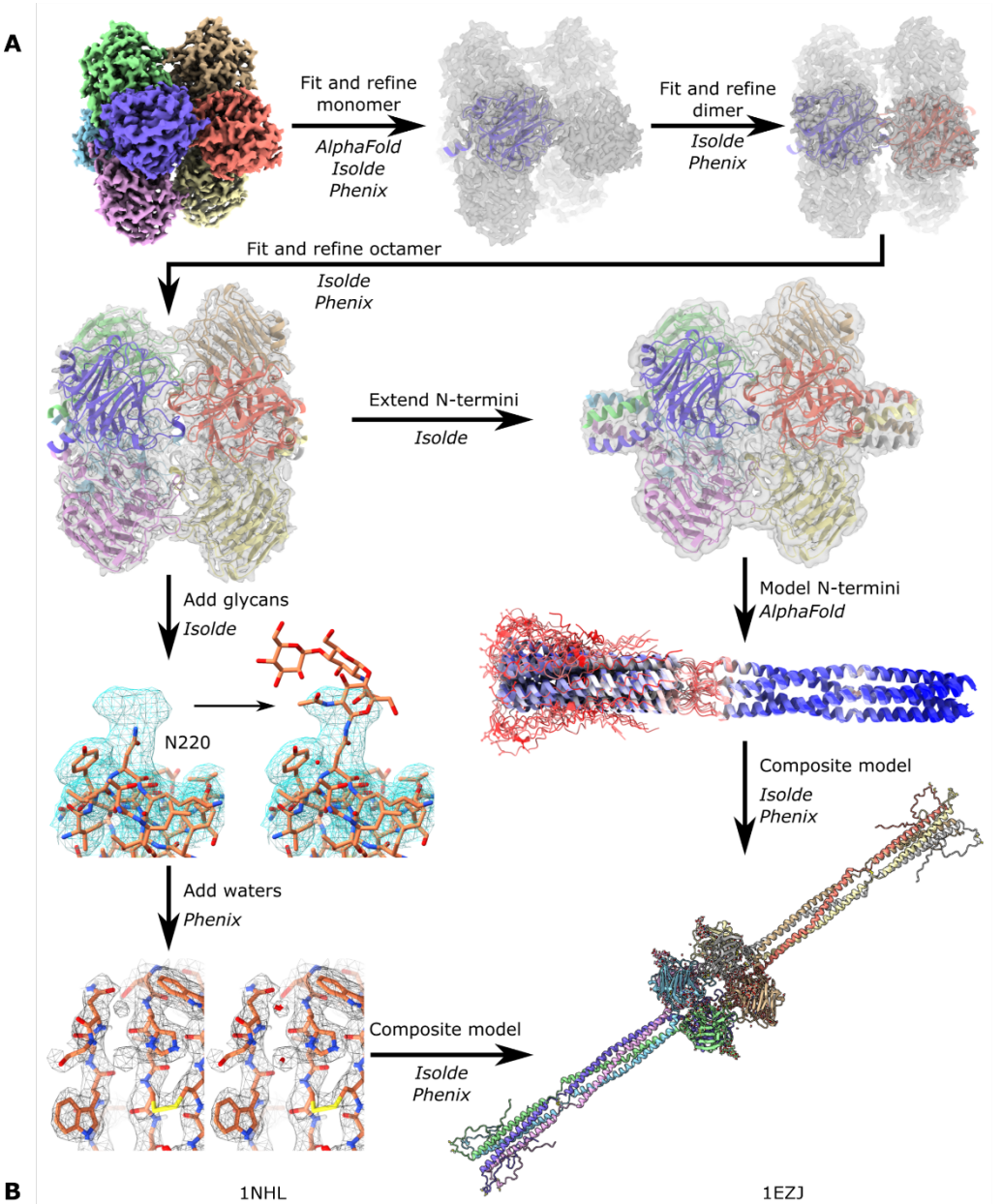
A
Fit and refine monomer
AlphaFold
Isolde
Phenix
Fit and refine dimer
Isolde
Phenix
Fit and refine octamer
Isolde
Phenix
Extend N-termini
Isolde
Add glycans
Isolde
N220
Model N-termini
AlphaFold
Composite model
Isolde
Phenix
Add waters
Phenix
Composite model
Isolde
Phenix
B
1NHL
1EZJ

Figure S6. Modelling of PTX3 atomic model using Isolde and AlphaFold, as well as AlphaFold outputs for the N-terminal domain of PTX3. (**A**) Pentraxin domains from AlphaFold derived PTX3 monomers as starting models for model refinement and energy minimisation in ISOLDE and Phenix. These were then scaled up to dimers, tetramers and then the octamers respectively. Density not accommodated by the electron density included N-linked glycans, of which a minimal carbohydrate structure of two N-acetylglucosamine and three mannose residues were added. Ordered water molecules were also appended to the model. The C-terminal proximal part of the N-terminal tail was modelled into the EM density as described above. This was extended using the rest of the predicted structure in AlphaFold and subsequently refined in Isolde and PHENIX resulting in a final composite model. (**B**) Representative AlphaFold outputs using seed sequences from 1NHL (5) and 1EZJ (6) (PDB entries). Models are coloured by confidence of the AlphaFold prediction, blue showing areas of high confidence and red showing those of low confidence. Prolines are highlighted as spheres.

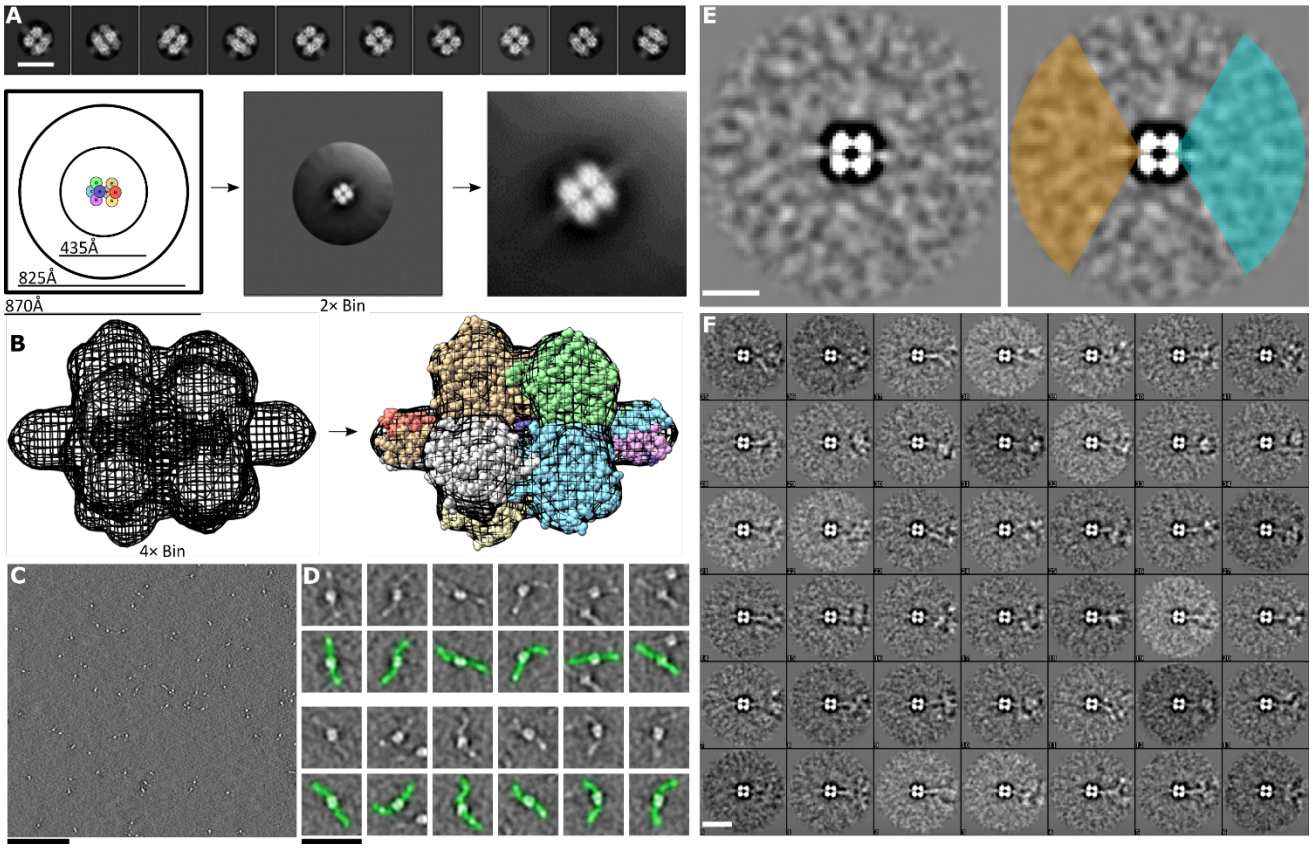

Figure S7. Dynamic masking, negative stain tomography and 2D variability analysis of cryoEM class averages to visualise the N-terminal region of PTX3. (**A**) 2D classes with a lower resolution region protruding from the PTX core corresponding to the N-terminal region (upper panel). Conventional 2D classification with extended box, background and mask sizes (870, 825 and 435 Å respectively) with 2×binning (lower panel). (**B**) 3D refinements with the same particle dimensions with 4× binning applied. (**C**) Negative stain tomogram of pure PTX3. (**D**) Enlarged individual PTX3 octamers from **C** with N-terminal regions. Density corresponding to PTX3 are highlighted in green. (**E**) Particles from within the classes such as those shown in **A** were aligned (*left*) and then subjected to 2D variability analysis in EMAN2 by aligning within the regions shown in orange and/or cyan (*right*). (**F**) Representative class averages, some of which display flexible tails protruding from the PTX domain core. Scale bars in (**C**), (**D**), (**E**) and (**F**) represent 200, 50, 10 and 20 nm respectively.

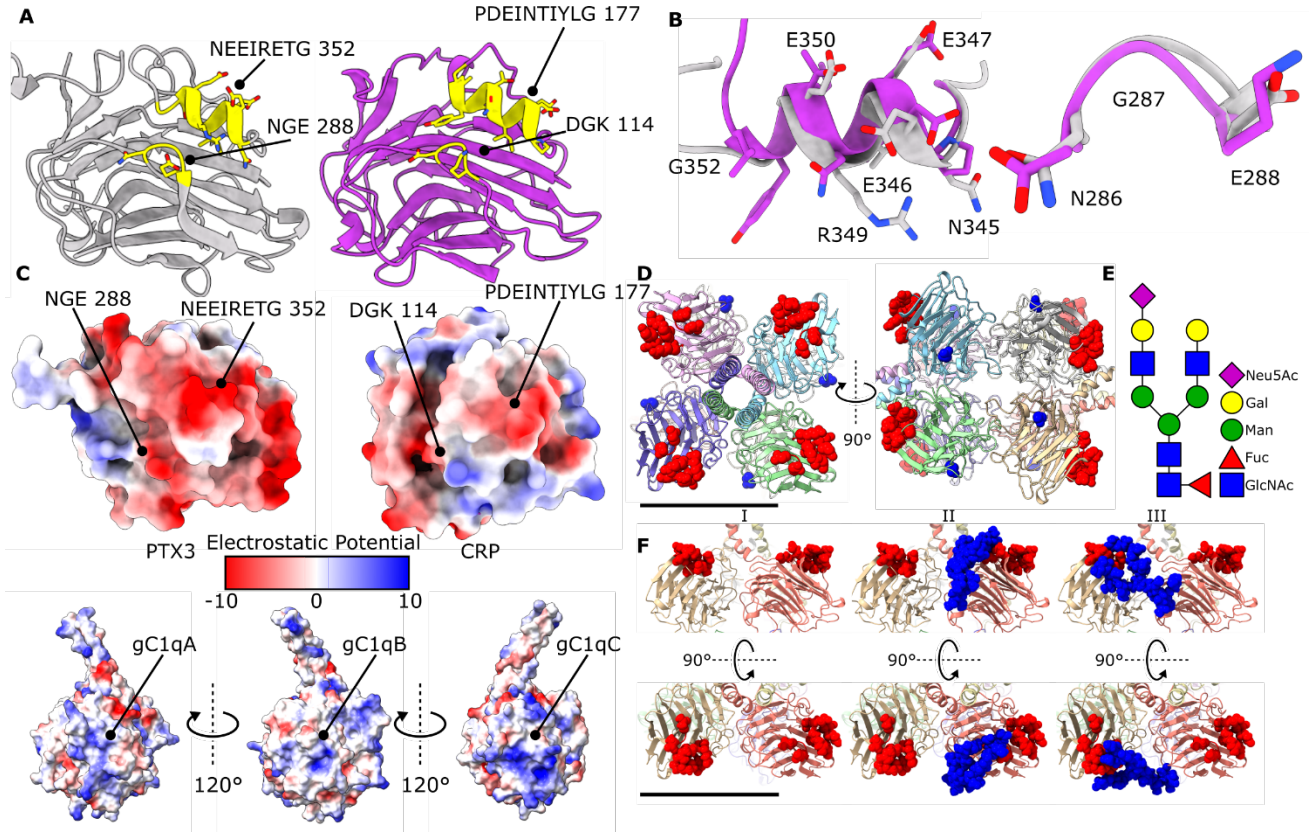

Figure S8. Identification of a putative C1 binding site in PTX3 and a structural basis for its inhibition by the N-linked carbohydrate moiety at N220. (**A**) Putative C1q binding site (yellow) compared between PTX3 (grey) and CRP (purple), with the constituent amino acids labelled. (**B**) Enlarged view of the α-helix and loop components of the CRP (purple) binding site and PTX3 (grey) putative binding site, with PTX3 numbering used. (**C**) Electrostatic surface of PTX3 and CRP (upper panel) as well as the globular head domain of C1q (gC1q, lower panel) shown, with the α-helix and loops region labelled on the pentraxins. Blue represents positive and red negative charge as shown in the electrostatic potential key that applies to both the pentraxins and gC1q. (**D**) Location of the putative C1 binding site (red spheres) and site of N-linked glycosylation, N220 (blue spheres). Schematic of the glycan added to N220 in Isolde shown; a biantennary sialylated glycan comprised of five N-acetylglucosamine (GlcNAc), three mannose units (Man), two galactoses (gal), a single fucose (Fuc) and one terminal sialic acid (Neu5Ac), which was one of the complex glycans identified by MS (**Fig. 4B,C**). (**E**) Modelling of this N220 linked carbohydrate moiety onto PTX3 (blue spheres). Views shown with no glycan present (I), a carbohydrate interacting with the C1 binding site on the same subunit (II) and a glycan interacting with the C1 binding site on a neighboring subunit (III). Scale bar in (**D**) and (**E**) represents 50 Å. Sialic acid, galactose, mannose, fucose and N-acetylglucosamine are represented by Neu5Ac, Gal, Man, Fuc and GlcNAc, respectively.

Table S1. Kinetic parameters from octet experiments using biotinylated PTX3 and full C1 complex.

Octet PTX3-C1 Complex Kinetic Parameters Global Fit	
K_D (M)	1.74e-8 (±1.04e-9)
K_{on} (1/ms)	4.8e6 (±2.73e5)
K_{off}	8.33e-2 (±1.58e-3)
R Square	0.970133

Table S2. Parameters and validation statistics for cryoEM data collection, reconstruction refinement and corresponding atomic models. *Model based on D4 symmetrized map.

Data collection		
Microscope	Titan Krios	
Camera	Gatan K3 detector	
Magnification	×105,000	
Voltage (kV)	300	
No. of frames	50	
Electron exposure (e–/Å^2)	50	
Defocus range (μm)	-0.8 to -2.4	
Pixel size (Å)	0.836	
Data processing		
No. of micrographs	4612	
No. of total particles	1,360,284	
No. of final particles	276,374	
Symmetry imposed	D4	C1
EMDB accession code	14774	14775
PDB accession code (cryoEM model)	7ZL1	N/A
Map resolution (FSC = 0.143) (Å)	2.5	2.8
Map resolution range (Å)	2.4-4.9	2.7-5.7
Map sharpening B factor (Å^2)	-73	-65
Refinement*		
Model resolution (FSC = 0.5) (Å)	2.5	
Model composition		
No. of nonhydrogen atoms	14,059	
No. of amino acid residues	1,720	
No. of ligands	40	
No. of waters	379	
B-factors (Å^2)		
Protein	35.98	

Ligands	77.86
Water	33.42
RMSD	
Bond lengths (Å)	0.007
Bond angles (°)	0.831
Validation	
MolProbity score	1.80
Clash score	4.28
Rotamer outliers (%)	1.58
Ramachandran plot	
Favored (%)	93.08
Allowed (%)	5.99
Disallowed (%)	0.94
Map to Model Average Map Value	
D4	0.03205
C1	0.02271
D4 map to C1 map cross correlation	0.9605

Table S3. BLAST sequence alignment of PTX3 and CRP comparing the human pentraxin sequence, the C317 and C318 disulfide path in PTX3 with the CRP Ca^{2+} binding loop and a putative C1q binding site. Conserved and conservative residues are respectively represented by "*" and ":".

Pentraxin sequences.

```
PTX3  HLCGTWNS 276
CRP   HICTSWES 102
SAP   HICVSWES 100
NPTX1 HICVTWTT 321
      *:* :* :
```

Disulfide patch (C317/C318) and the CRP Ca^{2+} binding loop.

```
PTX3  GQEKNGCCVGGGFD 324
CRP   GQEQ--DSFGGNFE 147
      ***:    .**.*:
```

Putative C1 binding site in PTX3 with C1 binding site in CRP.

α-helix

```
PTX3  NEEIRET--G 352
CRP   PDEINTIYLG 177
       :**.    *
```

Loop

```
PTX3  NGE 288
CRP   DGK 114
      :*:
```

Table S4. PTX3 glycopeptides identified by LC-MS/MS and Byonic searches, filtered for matches with a Byonic score >300.

Peptide	Glycan	Observed m/z	Charge	Observed (M+H)	Mass error (ppm)	Score	Protein Name	Band	Scan Time (min)
K.ATDVLN[+1298.476]K.T	HexNAc(4)Hex(3)	1029.9533	2	2058.8993	1.6	314	PTX3	1	21.1
K.ATDVLN[+1095.397]K.T	HexNAc(3)Hex(3)	928.4128	2	1855.8184	1	319	PTX3	1	21.2
K.ATDVLN[+1216.423]K.T	HexNAc(2)Hex(5)	988.9263	2	1976.8453	1.3	341	PTX3	1	21.0
K.ATDVLN[+1378.476]K.T	HexNAc(2)Hex(6)	1069.9523	2	2138.8974	0.8	366	PTX3	1	20.8
K.ATDVLN[+892.317]K.T	HexNAc(2)Hex(3)	826.873	2	1652.7387	0.9	370	PTX3	1	21.2
K.ATDVLN[+1702.581]K.T	HexNAc(2)Hex(8)	1232.006	2	2463.0048	1.4	380	PTX3	1	20.5
K.ATDVLN[+1378.476]K.T	HexNAc(2)Hex(6)	1069.9523	2	2138.8974	0.8	393	PTX3	1	20.8
K.ATDVLN[+1054.370]K.T	HexNAc(2)Hex(4)	907.8991	2	1814.7909	0.5	421	PTX3	1	21.0
K.ATDVLN[+892.317]K.T	HexNAc(2)Hex(3)	826.873	2	1652.7387	0.9	421	PTX3	1	21.2
K.ATDVLN[+203.079]K.T	HexNAc(1)	482.2534	2	963.4996	0.3	431	PTX3	1	21.4
K.ATDVLN[+1216.423]K.T	HexNAc(2)Hex(5)	988.9263	2	1976.8453	1.3	443	PTX3	1	21.0
K.ATDVLN[+1241.454]K.T	HexNAc(3)Hex(3)Fuc(1)	1001.4417	2	2001.8761	0.8	444	PTX3	1	21.2
K.ATDVLN[+1444.534]K.T	HexNAc(4)Hex(3)Fuc(1)	1102.9816	2	2204.9559	1	457	PTX3	1	21.1
K.ATDVLN[+1444.534]K.T	HexNAc(4)Hex(3)Fuc(1)	1102.9816	2	2204.9559	1	462	PTX3	1	21.1
K.ATDVLN[+349.137]K.T	HexNAc(1)Fuc(1)	555.2825	2	1109.5577	0.4	466	PTX3	1	21.5
K.ATDVLN[+1054.370]K.T	HexNAc(2)Hex(4)	907.8991	2	1814.7909	0.5	477	PTX3	1	21.0
K.ATDVLN[+1241.454]K.T	HexNAc(3)Hex(3)Fuc(1)	1001.4417	2	2001.8761	0.8	511	PTX3	1	21.2
K.ATDVLN[+203.079]K.T	HexNAc(1)	482.2534	2	963.4996	0.3	562	PTX3	1	21.4
K.ATDVLN[+349.137]K.T	HexNAc(1)Fuc(1)	555.2825	2	1109.5577	0.4	590	PTX3	1	21.5
K.ATDVLN[+349.137]KTILFSYGTK.R	HexNAc(1)Fuc(1)	707.373	3	2120.1043	1.6	343	PTX3	1	33.7
K.ATDVLN[+1444.534]KTILFSYGTK.R	HexNAc(4)Hex(3)Fuc(1)	1072.5041	3	3215.4976	0	486	PTX3	1	32.9
K.ATDVLN[+1241.454]KTILFSYGTK.R	HexNAc(3)Hex(3)Fuc(1)	1004.8111	3	3012.4188	0.2	504	PTX3	1	33.0
K.ATDVLN[+203.079]KTILFSYGTK.R	HexNAc(1)	658.6864	3	1974.0447	0.9	602	PTX3	1	34.0
K.ATDVLN[+1216.423]KTILFSYGTK.R	HexNAc(2)Hex(5)	996.467	3	2987.3865	0	719	PTX3	1	33.0
K.ATDVLN[+1216.423]KTILFSYGTK.R	HexNAc(2)Hex(5)	996.467	3	2987.3865	0	746	PTX3	1	33.0
K.ATDVLN[+1216.423]KTILFSYGTKR.N	HexNAc(2)Hex(5)	1048.5017	3	3143.4907	1	349	PTX3	1	31.0
K.ATDVLN[+1241.454]KTILFSYGTKR.N	HexNAc(3)Hex(3)Fuc(1)	792.8858	4	3168.5212	0.6	375	PTX3	1	31.1
K.ATDVLN[+1216.423]KTILFSYGTKR.N	HexNAc(2)Hex(5)	786.6281	4	3143.4905	0.9	490	PTX3	1	31.0
K.ATDVLN[+1216.423]KTILFSYGTKR.N	HexNAc(2)Hex(5)	1048.5017	3	3143.4907	1	603	PTX3	1	31.0
K.ATDVLN[+1216.423]KTILFSYGTKR.N	HexNAc(2)Hex(5)	786.6281	4	3143.4905	0.9	699	PTX3	1	31.0
K.ATDVLN[+2715.963]K.T	HexNAc(5)Hex(6)Fuc(1)NeuAc(2)	1159.4666	3	3476.3853	0.8	312.7	PTX3	2	22.4
K.ATDVLN[+1444.534]K.T	HexNAc(4)Hex(3)Fuc(1)	1102.9815	2	2204.9557	0.9	316.9	PTX3	2	21.0
K.ATDVLN[+1768.640]K.T	HexNAc(4)Hex(5)Fuc(1)	843.6923	3	2529.0623	1.1	321.5	PTX3	2	20.9
K.ATDVLN[+1768.640]K.T	HexNAc(4)Hex(5)Fuc(1)	843.6923	3	2529.0623	1.1	322.5	PTX3	2	20.9
K.ATDVLN[+1809.666]K.T	HexNAc(5)Hex(4)Fuc(1)	1285.5478	2	2570.0883	0.9	323.6	PTX3	2	20.8
K.ATDVLN[+2424.867]K.T	HexNAc(5)Hex(6)Fuc(1)NeuAc(1)	1062.4351	3	3185.2907	1.1	325.7	PTX3	2	21.5
K.ATDVLN[+2424.867]K.T	HexNAc(5)Hex(6)Fuc(1)NeuAc(1)	1062.435	3	3185.2903	1	332.7	PTX3	2	21.3
K.ATDVLN[+1216.423]K.T	HexNAc(2)Hex(5)	988.9262	2	1976.8451	1.2	334.9	PTX3	2	20.9

K.ATDVLN[+1403.507]K.T	HexNAc(3)Hex(4)Fuc(1)	1082.4684	2	2163.9296	1.1	341.1	PTX3	2	21.0
K.ATDVLN[+2424.867]K.T	HexNAc(5)Hex(6)Fuc(1)NeuAc(1)	1062.435	3	3185.2903	1	342.4	PTX3	2	21.3
K.ATDVLN[+2350.830]K.T	HexNAc(4)Hex(5)Fuc(1)NeuAc(2)	1037.756	3	3111.2535	1	348.7	PTX3	2	22.5
K.ATDVLN[+1606.587]K.T	HexNAc(4)Hex(4)Fuc(1)	1184.0081	2	2367.0089	1	350.4	PTX3	2	20.8
K.ATDVLN[+2059.735]K.T	HexNAc(4)Hex(5)Fuc(1)NeuAc(1)	940.7241	3	2820.1579	1.1	356.7	PTX3	2	21.6
K.ATDVLN[+1768.640]K.T	HexNAc(4)Hex(5)Fuc(1)	1265.0348	2	2529.0624	1.2	390.8	PTX3	2	20.9
K.ATDVLN[+1606.587]K.T	HexNAc(4)Hex(4)Fuc(1)	1184.0081	2	2367.0089	1	416.4	PTX3	2	20.8
K.ATDVLN[+1768.640]K.T	HexNAc(4)Hex(5)Fuc(1)	1265.0348	2	2529.0624	1.2	455.9	PTX3	2	20.9
K.ATDVLN[+2350.830]K.T	HexNAc(4)Hex(5)Fuc(1)NeuAc(2)	1037.756	3	3111.2535	1	466.2	PTX3	2	22.5
K.ATDVLN[+1606.587]KTILFSYGTK.R	HexNAc(4)Hex(4)Fuc(1)	1126.5229	3	3377.554	1.1	319.0	PTX3	2	32.6
K.ATDVLN[+2133.772]KTILFSYGTK.R	HexNAc(5)Hex(6)Fuc(1)	1302.2513	3	3904.7393	1	391.4	PTX3	2	32.3
K.ATDVLN[+2424.867]KTILFSYGTK.R	HexNAc(5)Hex(6)Fuc(1)NeuAc(1)	1399.2836	3	4195.8363	1.3	394.7	PTX3	2	33.8
K.ATDVLN[+1971.719]KTILFSYGTK.R	HexNAc(5)Hex(5)Fuc(1)	1248.2335	3	3742.6858	0.9	410.4	PTX3	2	32.5
K.ATDVLN[+2424.867]KTILFSYGTK.R	HexNAc(5)Hex(6)Fuc(1)NeuAc(1)	1399.2836	3	4195.8363	1.3	418.5	PTX3	2	33.8
K.ATDVLN[+1971.719]KTILFSYGTK.R	HexNAc(5)Hex(5)Fuc(1)	1248.2335	3	3742.6858	0.9	455.4	PTX3	2	32.5
K.ATDVLN[+2059.735]KTILFSYGTK.R	HexNAc(4)Hex(5)Fuc(1)NeuAc(1)	1277.5727	3	3830.7035	1.3	476.4	PTX3	2	34.1
K.ATDVLN[+1606.587]KTILFSYGTK.R	HexNAc(4)Hex(4)Fuc(1)	1126.5229	3	3377.554	1.1	527.3	PTX3	2	32.6
K.ATDVLN[+2059.735]KTILFSYGTK.R	HexNAc(4)Hex(5)Fuc(1)NeuAc(1)	1277.5724	3	3830.7028	1.1	698.4	PTX3	2	33.9
K.ATDVLN[+2100.761]KTILFSYGTK.R	HexNAc(5)Hex(4)Fuc(1)NeuAc(1)	1291.2477	3	3871.7287	0.9	708.9	PTX3	2	34.0
K.ATDVLN[+2100.761]KTILFSYGTK.R	HexNAc(5)Hex(4)Fuc(1)NeuAc(1)	1291.2477	3	3871.7287	0.9	711.7	PTX3	2	34.0
K.ATDVLN[+1768.640]KTILFSYGTK.R	HexNAc(4)Hex(5)Fuc(1)	1180.5406	3	3539.6072	1.1	715.9	PTX3	2	32.6
K.ATDVLN[+1768.640]KTILFSYGTK.R	HexNAc(4)Hex(5)Fuc(1)	1180.5406	3	3539.6072	1.1	761.4	PTX3	2	32.6
K.ATDVLN[+2059.735]KTILFSYGTK.R	HexNAc(4)Hex(5)Fuc(1)NeuAc(1)	1277.5724	3	3830.7028	1.1	772.8	PTX3	2	33.9
K.ATDVLN[+1809.666]KTILFSYGTKR.N	HexNAc(5)Hex(4)Fuc(1)	934.9389	4	3736.7337	0.8	307.8	PTX3	2	30.7
K.ATDVLN[+3007.058]KTILFSYGTKR.N	HexNAc(5)Hex(6)Fuc(1)NeuAc(3)	1234.0364	4	4933.1238	0.9	309.5	PTX3	2	34.7
K.ATDVLN[+2350.830]KTILFSYGTKR.N	HexNAc(4)Hex(5)Fuc(1)NeuAc(2)	1426.6367	3	4277.8954	0.1	310.9	PTX3	2	33.4
K.ATDVLN[+1809.666]KTILFSYGTKR.N	HexNAc(5)Hex(4)Fuc(1)	934.9389	4	3736.7337	0.8	325.1	PTX3	2	30.7
K.ATDVLN[+2100.761]KTILFSYGTKR.N	HexNAc(5)Hex(4)Fuc(1)NeuAc(1)	1007.7127	4	4027.8289	0.7	408.7	PTX3	2	32.0
K.ATDVLN[+2133.772]KTILFSYGTKR.N	HexNAc(5)Hex(6)Fuc(1)	1015.9653	4	4060.8392	0.7	429.2	PTX3	2	30.5
K.ATDVLN[+2350.830]KTILFSYGTKR.N	HexNAc(4)Hex(5)Fuc(1)NeuAc(2)	1070.2303	4	4277.8992	1	431.7	PTX3	2	33.5
K.ATDVLN[+1768.640]KTILFSYGTKR.N	HexNAc(4)Hex(5)Fuc(1)	924.6826	4	3695.7086	1.2	448.8	PTX3	2	30.6
K.ATDVLN[+2100.761]KTILFSYGTKR.N	HexNAc(5)Hex(4)Fuc(1)NeuAc(1)	1007.7127	4	4027.8289	0.7	467.9	PTX3	2	32.0
K.ATDVLN[+2350.830]KTILFSYGTKR.N	HexNAc(4)Hex(5)Fuc(1)NeuAc(2)	1070.2303	4	4277.8992	1	476.2	PTX3	2	33.5
K.ATDVLN[+3007.058]KTILFSYGTKR.N	HexNAc(5)Hex(6)Fuc(1)NeuAc(3)	1234.0364	4	4933.1238	0.9	486.4	PTX3	2	34.7
K.ATDVLN[+2059.735]KTILFSYGTKR.N	HexNAc(4)Hex(5)Fuc(1)NeuAc(1)	997.4562	4	3986.803	0.8	517.5	PTX3	2	31.9
K.ATDVLN[+1768.640]KTILFSYGTKR.N	HexNAc(4)Hex(5)Fuc(1)	924.6826	4	3695.7086	1.2	539.7	PTX3	2	30.6
K.ATDVLN[+2100.761]KTILFSYGTKR.N	HexNAc(5)Hex(4)Fuc(1)NeuAc(1)	1007.7127	4	4027.8289	0.7	541.6	PTX3	2	32.0
K.ATDVLN[+2059.735]KTILFSYGTKR.N	HexNAc(4)Hex(5)Fuc(1)NeuAc(1)	997.4562	4	3986.803	0.8	563.3	PTX3	2	31.9
K.ATDVLN[+2350.830]KTILFSYGTKR.N	HexNAc(4)Hex(5)Fuc(1)NeuAc(2)	1070.2303	4	4277.8992	1	567.4	PTX3	2	33.5
K.ATDVLN[+2059.735]KTILFSYGTKR.N	HexNAc(4)Hex(5)Fuc(1)NeuAc(1)	997.4562	4	3986.803	0.8	606.8	PTX3	2	31.9

Table S5. Coiled coil oligomeric state prediction and register assignment, as well as fusion sequences of N-terminal residues of PTX3 (underlined) with sequences of known tetrameric coiled-coil structures. The sequence for the N-terminal region was assessed using Logicoil (7), which predicted the oligomeric state as a tetramer and assigned the heptad repeat (denoted *abcdefg*). Fusion proteins of the N-terminal region of PTX3 with known coiled coil proteins, 1NHL (5) and 1EZJ (6), with residues corresponding to *a* and *d* positions within the heptad repeat highlighted in bold as determined by Logicoil (7).

PTX3 N-terminal coiled coil predictions

Sequence	60	FIMLENSQMRERMLLQATDDVLRGELQRLREELGRLAESL
Register		defgabcdefgabcdefgabcdefgabcdefgabcdefga
Sequence	100	ARPCAPGAPAEARLTSALDELLQATRDAGRRLARMEGAEA
Register		bcdefgabcdefgabcdefgabcdefgabcdefgabcdef
Sequence	140	QRPEEAGRALAAVLEELRQTRADLHAVQGWAAR
Register		ggabcdefgabcdefgabcdefgabcdefgabc

Fusion sequence PTX3+1NHL:

ENSDDYDLMYVNLDNEIDNGLHPTEDPTPCACGQEHSEWDKLFIMLENSQMRERMLLQAT
DDVLRGELQRLREELGRLAESLARPCAPGAPAEARLTSALDELLQATRDAGRRLARMEGA
EAQRPEEAGRA**L**AA**V**LEE**L**RQ**T**RAD**L**HA**V**QGW**T**RR**I**LGL**A**IE**S**QDA**G**IK**T**ITM**L**DE**Q**KEQ
LNR**I**EEG**L**DQ**I**NKD**M**RE**T**EKT**L**TE**L**

Fusion sequence PTX3+1EZJ:

ENSDDYDLMYVNLDNEIDNGLHPTEDPTPCACGQEHSEWDKLFIMLENSQMRERMLLQAT
DDVLRGELQRLREELGRLAESLARPCAPGAPAEARLTSALDELLQATRDAGRRLARMEGA
EAQRPEEAGRA**L**AA**V**LEE**L**RQ**T**RAD**L**HA**V**CGL**I**LS**A**EKS**S**ARK**V**DE**N**KQL**L**KQ**I**QES**V**ES
FRDI**Y**KR**F**SEY**Q**KEQ**N**SL**L**MSN**L**STLHIITD

Table S6. Full-length sequence of secreted PTX3 showing regions where structure determination was performed using cryoEM (double underline) or AlphaFold (dotted underline).

ENSDDYDLMYVNLDNEIDNGLHPTEDPTPCACGQEHSEWDKLFIMLENSQMRERMLLQAT
DDVLRGELQRLREELGRLAESLARPCAPGAPAEARLTSALDELLQATRDAGRRLARMEGA
EAQRPEEAGRALAAVLEELRQTRADLHAVQGWAARSWLPAGCETAILFPMRSKKIFGSVH
PVRPMRLESFSACIWVKATDVLNKTILFSYGTKRNPYEIQLYLSYQSIVFVVGGEENKLV
AEAMVSLGRWTHLCGTWNSEEGLTSLWVNGELAATTVEMATGHIVPEGGILQIGQEKNGC
CVGGGFDETLAFSGRLTGFNIWDSVLSNEEIRETGGAESCHIRGNIVGWGVTEIQPHGGA
QYVS

Table S7. Known ligands of PTX3 and their likely interaction domains on PTX3. *C1q based on homology modelling with residues shown to be important in CRP for C1 binding and complement activation. †VEGF also binds to PTX3, likely via a similar mechanism, but with lower affinity. ‡The monoclonal antibody MNB4 binds to this site and inhibits PTX3-inter-α-trypsin association, as such, steric hinderance of an adjacent site cannot be ruled out.

Ligand	PTX3 Binding Domain	PTX3 Residues	Biological Function	Reference
C1q*	*C-term*	*286-288, 345-352*	*Complement activation*	*(8-10)*
Fcγ receptors	*C-term*	*Unknown*	*Phagocytosis*	*(11)*
Haemagglutinin	*C-term*	*Sialylation at N220*	*Anti-viral*	*(12)*
P-selectin	*C-term*	*Sialylation at N220*	*Leukocyte regulation*	*(13)*
Ficolins (1,2,3,M,L & H)	*C-term*	*Glycosylation at N220*	*Anti-fungal & complement activation*	*(14, 15)*
Factor H	*C-term & N-term*	*N-term and glycosylation at N220*	*Complement regulation*	*(16)*
C4b-binding protein	*C-term*	*C1q binding site*	*Complement regulation*	*(17)*
FGF2†	*N-term*	*97-110*	*Angiogenesis, would healing & cell growth*	*(18, 19)*
TSG6	*N-term*	*FGF2 binding site*	*Female fertility*	*(20)*
Inter-α-trypsin‡	*N-term*	*87-99*	*Female fertility*	*(21)*
Histone	*N-term*	*Unknown*	*Neutrophil extracellular trap regulation*	*(22)*
OmpA	*Unknown*	*Unknown*	*Anti-bacterial*	*(23)*
MHV	*Unknown*	*Unknown*	*Anti-viral*	*(24)*
MBL	*Unknown*	*Unknown*	*Complement activation*	*(25, 26)*
Zymosan	*Unknown*	*Unknown*	*Anti-fungal*	*(27)*

3 Supplementary References

1. Tegunov D & Cramer P Real-time cryo-electron microscopy data preprocessing with Warp. *Nature Methods* 16(11):1146-1152 (2019).
2. Bell J, M., Chen M, Durmaz T, Fluty A, C. , & Ludtke S, J. New software tools in EMAN2 inspired by EMDatabank map challenge. *Journal of Structural Biology* 204(2):283-290 (2018).
3. Scheres S, H. W. Amyloid structure determination in RELION-3.1. *Acta Crystallographica. Section D, Structural Biology* 76(1):94-101 (2020).
4. Pettersen E, F*., et al.* UCSF ChimeraX: Structure visualization for researchers, educators, and developers. *The Protein Society* 30(1):70-82 (2021).
5. Freedman SJ, Song HK, Xu Y, Sun Z-YJ, & Eck MJ Homotetrameric Structure of the SNAP-23 N-terminal Coiled-coil Domain. *Journal of Biological Chemistry* 278(15):13462-13467 (2003).
6. Tarbouriech N, Curran J, Ruigrok RWH, & Burmeister WP Tetrameric coiled coil domain of Sendai virus phosphoprotein. *Nature Structural Biology* 7(9):777-781 (2000).
7. Vincent TL, Green PJ, & Woolfson DN LOGICOIL—multi-state prediction of coiled-coil oligomeric state. *Bioinformatics (Oxford, England)* 29(1):69-76 (2012).
8. Bottazzi B*, et al.* Multimer formation and ligand recognition by the long pentraxin PTX3. Similarities and differences with the short pentraxins C-reactive protein and serum amyloid P component. *J Biol Chem* 272(52):32817-32823 (1997).
9. Bang R*, et al.* Analysis of Binding Sites in Human C-reactive Protein for FcγRI, FcγRIIA, and C1q by Site-directed Mutagenesis. *The Journal of Biological Chemistry* 280(26):25095-25102 (2005).
10. Alok A & John EV Probing the C1q-binding site on human C-reactive protein by site-directed mutagenesis. *The Journal of Immunology* 1(152):5404-5410 (1994).
11. Lu J*, et al.* Structural recognition and functional activation of FcγR by innate pentraxins. *Nature* 456(7224):989-992 (2008).
12. Reading P, C*., et al.* Antiviral activity of the long chain pentraxin PTX3 against influenza viruses. *J Immunol* 180(5) (2008).
13. Deban L*, et al.* Regulation of leukocyte recruitment by the long pentraxin PTX3. . *Nat Immunol.* 11(4):328-334 (2010).
14. Gout E*, et al.* M-ficolin interacts with the long pentraxin PTX3: a novel case of cross-talk between soluble pattern-recognition molecules. *J Immunol.* 186(10):5815-5822 (2011).
15. Visser CA Synergy between ficolin-2 and pentraxin 3 boosts innate immune recognition and complement deposition. . *J Biol Chem.* 284(41):28263-28275 (2009).
16. Deban L*, et al.* Binding of the long pentraxin PTX3 to factor H: interacting domains and function in the regulation of complement activation. *J Immunol* 181(12):8433-8440 (2008).
17. Braunschweig A & Józsi M Human pentraxin 3 binds to the complement regulator c4b-binding protein. *PloS one* 6(8):e23991-e23991 (2011).

18. Camozzi M*, et al.* Identification of an antiangiogenic FGF2-binding site in the N terminus of the soluble pattern recognition receptor PTX3. *J Biol Chem* 281(32):22605-22613 (2006).

19. Inforzato A*, et al.* The angiogenic inhibitor long pentraxin PTX3 forms an asymmetric octamer with two binding sites for FGF2. *J Biol Chem* 285(23):17681-17692 (2020).

20. Leali D*, et al.* Long pentraxin 3/tumor necrosis factor-stimulated gene-6 interaction: a biological rheostat for fibroblast growth factor 2-mediated angiogenesis. *Arterioscler Thromb Vasc Biol* 32(3):696-703 (2012).

21. Scarchilli L CA, Bottazzi B, Negri V, Doni A, Deban L, Bastone A, Salvatori G, Mantovani A, Siracusa G, Salustri A. PTX3 interacts with inter-alpha-trypsin inhibitor: implications for hyaluronan organization and cumulus oophorus expansion. *J Biol Chem* 282(41):30161-30170 (2007).

22. Daigo K, Takamatsu Y, & Hamakubo T The Protective Effect against Extracellular Histones Afforded by Long-Pentraxin PTX3 as a Regulator of NETs. 7(344) (2016).

23. Jeannin P*, et al.* Complexity and complementarity of outer membrane protein A recognition by cellular and humoral innate immunity receptors. *Immunity* 22(5):551-560 (2005).

24. Han B*, et al.* Protective effects of long pentraxin PTX3 on lung injury in a severe acute respiratory syndrome model in mice. *Laboratory investigation; a journal of technical methods and pathology* 92(9):1285-1296 (2012).

25. Ma Y, Jie*, et al.* Heterocomplexes of Mannose-binding Lectin and the Pentraxins PTX3 or Serum Amyloid P Component Trigger Cross-activation of the Complement System. *Journal of Biological Chemistry* 286(5):3405-3417 (2011).

26. Stallone G*, et al.* Modulation of complement activation by pentraxin-3 in prostate cancer. *Scientific Reports* 10(1):18400 (2020).

27. Diniz SN*, et al.* PTX3 function as an opsonin for the dectin-1-dependent internalization of zymosan by macrophages. *J Leukoc Biol* 75(4):649-656 (2004).